Optics and Lasers in Engineering 55 (2014) 221–225

Contents lists available at ScienceDirect

Optics and Lasers in Engineering

journal homepage: www.elsevier.com/locate/optlaseng

Simple wavelength-to-phase mapping FBG's interrogation method

Alejandro A. Giordana [a,*], Enrique E. Sicre [b], Ricardo Duchowicz [a,c]

[a] Centro de Investigaciones Ópticas (CIOp), P.O. Box 3, 1897 Gonnet, La Plata, Argentina
[b] Instituto de Tecnología, UADE, Lima 775, 1073 CABA, Argentina
[c] Facultad de Ingenieria, Universidad Nacional de La Plata, 1 y 47, La Plata, Argentina

ARTICLE INFO

Article history:
Received 19 June 2013
Received in revised form
8 October 2013
Accepted 18 November 2013

Keywords:
Optical fiber
Sensor
Bragg grating
Optical interrogator
Phase detection

ABSTRACT

In this work, an interrogation method for FBG sensors is presented based on a wavelength-to-time transformation procedure. The proposed scheme uses an externally modulated broadband source, an optical circulator and three Bragg gratings fixed in three different fiber branches, one acting as sensor (FBG_S) and others two (FBG_1 and FBG_2) acting as wavelength calibration devices. Spectral positions of the reflectivity maximum of $FBG_{1,2}$ are slightly different and fixed while FBG_S spectral position lies in the reflection spectral range of $FBG_{1,2}$. Moreover, an optical time delay between the reflections of both calibration gratings is introduced including a path length greater in one of the branches. Reflections from both gratings are added by employing a 50/50 coupler. By this set-up, a phase sensible detection technique is generated allowing to reach a sensitivity of up to 660°/nm in the performed experiments. A theoretical analysis of the device performance was carried out showing good agreement with the experimental results. This system combines low cost and high flexibility to be customized in a particular application.

1. Introduction

Fiber Bragg Grating (FBG) sensors are widely used in several applications. Its electromagnetic interference immunity, high temperature endurance, small size, low insertion profile, embedded capability, multiplexing flexibility, among other features, have made possible a quite fast development spreading their employment in different fields.

Basically, the measuring capability of any sensor device based on FBG lies in the accurate determination of a wavelength shift. Four broad kinds of methods could be defined [1]: (a) static methods, (b) sweep methods, (c) interferometric methods and (d) methods based on dispersive systems. In the methods included in (a), optic element acting as wavelength-to-intensity traducer is needed, which use fix filters [2,3], edge filters or source spectral shape [4,5]. Case (b) involves sweeping methods that employ tunable Fabry–Perot filters or tunable laser sources [6]; case (c) takes advantage of the use of interferometric techniques [7,8] and in case (d) high frequency detection is achieved by using the so-called wavelength to time translation based on properties of several dispersive media [9,10].

Resolution vs. dynamic range trade-off is a common feature to any of the four kinds of measuring methods mentioned above. The last one seems to be one of the best due to the very short time required to monitor a FBG sensor system with high resolution and extended range. System complexity and "cost by sensor" are sensitive factors for this kind of interrogation technique to become practical or, even though, to reach the market. Moreover, each application has different requirements. Some of them do not require a huge dynamic range, but the frequency response is more important. For example, train traffic monitoring systems [11] show practical results using an interrogation system with only a 300 pm wavelength band. In other cases, high sensitivity could be required [12].

This work is based on two main references. In the first place, we used the same approach developed by Abad et al. [13], who proposed a very simple scheme that includes a double conversion interrogation technique: wavelength-to-amplitude and amplitude-to-phase conversion. In the second place, our proposal takes advantage of the customization flexibility demonstrated by Nunes et al. [2]. He analyzed the use of two FBG as fixed filters in a wavelength-to-amplitude translation based interrogator. The use of two fixed filters instead of one gives an additional degree of freedom for system implementation. It will be showed that varying the filters separation different ranges and sensitivities could be obtained. Therefore this method combines low cost and simplicity with high flexibility to be customized as required for a particular application.

2. Method

The setup is schematically shown in Fig. 1. The principle of operation is based on the transformation of a light wavelength

* Corresponding author. Tel.: +54 221 484 0280; fax: +54 221 471 2771.
E-mail address: agiordana@ciop.unlp.edu.ar (A.A. Giordana).
URL: http://www.ciop.unlp.edu.ar (A.A. Giordana).

0143-8166/$ - see front matter © 2013 Elsevier Ltd. All rights reserved.
http://dx.doi.org/10.1016/j.optlaseng.2013.11.010

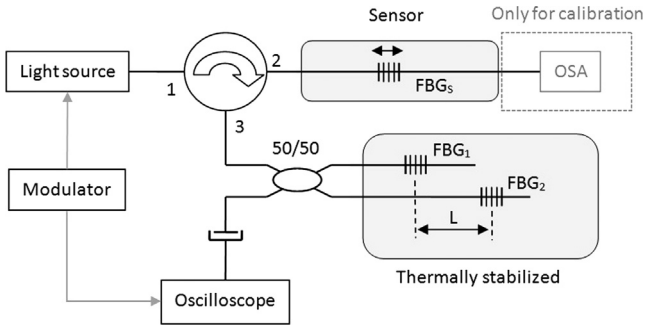

Fig. 1. Measuring and calibration scheme.

variation into an electrical phase change of the photodetected signal. The sensor grating (FBG$_S$) is illuminated with a broadband light source modulated at frequency f_c. The light reflected by FBG$_S$ is carried toward two calibrated FBG (FBG$_1$ and FBG$_2$) where a wavelength-to-amplitude conversion takes place. The reflected light beams from both gratings, b_1 and b_2, are time delayed proportionally to a path length difference L between the branches. Finally the intensities of b_1 and b_2 are added by employing a 50/50 coupler.

The goal of the presented method is to select the spectral positions of the gratings FBG$_1$ and FBG$_2$ in such a way to generate a relative intensity variation of b_1 and b_2 as a function of the sensor wavelength shift. As it is analytically shown in the next section by measuring the relative phase between the modulation and the photodetected signals it is possible to determine the FBG$_S$ wavelength. Fig. 5 shows an example where the peaks position of FBG$_1$ and FBG$_2$ are shifted by a certain amount $\Delta\lambda$, while the FBG$_S$ spectrum lies in the range where it is superimposed with the FBG$_1$ and FBG$_2$ reflection range. In this work, we consider $\Delta\lambda$ values lying between $\delta\lambda_{BG}/3$ to $1.5\delta\lambda_{BG}$, being $\delta\lambda_{BG}^{(i)}=\delta\lambda_{BG}$ the spectral widths of FBG$_i$ ($i=1,2$) which were assumed the same.

In order to obtain the amplitude-to-phase conversion the time delay is computed to generate a 90° phase shift at the modulation frequency; namely

$$L=\frac{c}{8f_c n_{eff}} \tag{1}$$

where c is the vacuum light speed and n_{eff} is the effective refractive index.

The method is based on two conversion steps; namely, wavelength-to-amplitude and amplitude-to-phase. Once the system has been calibrated, the accuracy is given by the long term stability of the magnitudes involved in both processes. Those are: the spectral shape and position of the calibrated FBG$_{1,2}$, the spectral shape of the sensor, the time delay between calibrated Bragg gratings, the coupler ratio and the spectral shape of the light source. Any change in these parameters would produce accuracy degradation.

The sensor wavelength is determined by measuring the phase of the photodetected signal relative to the modulation signal. Precision depends on the system signal to noise ratio (SNR). The final bandwidth that can be obtained is closely related to the phase detection algorithm, and as a consequence it is related to SNR. As a general rule if more modulation cycles are processed the bandwidth is reduced diminishing the noise and improving precision. On the other hand, if the bandwidth becomes smaller output data rate is also reduced.

The modulation frequency bounds the system maximum bandwidth. Therefore by choosing a high modulation frequency fast measurements could be done. In this case the system performance is limited by the light source and the photodetector frequency response.

The scheme shown in Fig. 1 was implemented as follows. A SLED (EXALOS – EXS1510-2101) coupled to SM fiber was used as light source capable to be modulated up to 30 MHz by using an electrical wave generator. SM standard fibers, an optical circulator and a 50:50 coupler were employed in the set-up. The photodetector (Thor-Labs 50 MHz) was connected to the oscilloscope (LeCroy-Wave Runner 610Zi) acting as the processing unit. The oscilloscope was synchronized with the wave generator in order to have a phase reference. A custom signal processing was implemented with oscilloscope's tools for performing the phase determination. The data sampling time interval is 5 μs but the time processing required by the algorithm to determine the signal phase shift gives rise to an output data rate of 1 Hz.

To implement the time delay a patch cord of ~3.2 m length was used. From Eq. (1) the frequency should be 7.8 MHz. However, in order to take advantage of the SLED and photodetector bandwidth, a 23.5 MHz modulation frequency was chosen. Actually, at this frequency, a 3.2 m patch cord introduces a phase shift of 270° which for the interrogation method it is equivalent to a relative 90° phase shift.

To control the FBG's spectral positions, a heating resistor was attached to each grating. An OSA (Yokogawa-AQ6370B) was used to measure the transmission spectrum of the sensor central wavelength. The system was characterized by measuring at the same instant the detected phase with the oscilloscope and the sensor central wavelength with the OSA, while the sensor wavelength was thermally swept with the heating resistor. Fig. 7 was obtained by plotting these pairs of data for different values of $\Delta\lambda$.

3. Theory

A Gaussian shape for the gratings reflectivity and a flat source emission spectrum in the region of interest are assumed. Same as in [8], we can express the spectral density of optical power reflected by FBG$_S$ when arriving to each FBG$_i$ as

$$D_i(t,\lambda,\lambda_s)=PSA_{tti}\exp(-\alpha_s(\lambda-\lambda_s)^2)\sin(\omega_c t+\gamma_i) \tag{2}$$

where

$$\alpha_s=\frac{4\ln 2}{\delta\lambda^2} \tag{3}$$

In Eqs. (2) and (3), P is the optical power density [W/nm], S is the FBG sensor reflectivity, A_{tt} is the fiber attenuation from FBG$_S$ to FBG$_i$, λ_s is the wavelength associated with the maximum of FBG$_S$ reflectivity, $\delta\lambda$ is the spectral width of the sensor (FWHM) and finally, γ_i is the phase shift associated with the optical path difference from FBG$_S$ to each FBG$_i$. After the light is reflected by FBG$_i$ (with $i=1$ and 2), the corresponding spectral density becomes

$$D_i(t,\lambda,\lambda_s)=PSF_iA_{tti}\exp(-\alpha_i(\lambda-\lambda_i)^2)\exp(-\alpha_s(\lambda-\lambda_s)^2)\sin(\omega_c t+\gamma+\varphi_i) \tag{4}$$

with

$$\alpha_i=\frac{4\ln 2}{\delta\lambda_i^2} \tag{5}$$

F_i being the reflectivity of FBG$_i$, $\delta\lambda_i$ the spectral width of the FBG$_i$ (FWHM) and φ_i the phase shift induced by the optical path from FBG$_i$ to the detector. The phase difference resulting from the two paths (corresponding to the beam reflected by FBG$_1$ or FBG$_2$) is

$$(\gamma_2+\varphi_2)-(\gamma_1+\varphi_1)=\theta \tag{6}$$

where the value of θ is given by

$$\theta=\frac{4\pi n_{eff}L}{c}f_c \tag{7}$$

Thus the optical intensity of the signal arriving to the photodetector becomes

$$I(t,\lambda_s)=\int_{-\infty}^{+\infty}(D_1(t,\lambda,\lambda_s)+D_2(t,\lambda,\lambda_s))\,d\lambda \tag{8}$$

By considering $\theta=\pi/2$ and that the only gratings difference concerns to their spectral positions (i.e., $F_1=F_2=F$), by replacing Eq. (4) in (8) it results

$$\begin{aligned} I(t,\lambda_s) &= B\int_{-\infty}^{+\infty}\exp(-\alpha_s(\lambda-\lambda_s)^2)\Big(\exp(-\alpha(\lambda-\lambda_1)^2)\sin(\omega_c t) \\ &\quad +\exp(-\alpha(\lambda-\lambda_2)^2)\sin(\omega_c t-\pi/2)\Big)\,d\lambda \\ &= B\sqrt{\frac{\pi}{2\alpha}}\Big(\exp\Big(-\frac{\alpha}{2}(\lambda_s-\lambda_1)\Big)^2)\sin(\omega_c t) \\ &\quad +\exp\Big(-\frac{\alpha}{2}(\lambda_s-\lambda_2)^2\Big)\cos(\omega_c t)\Big) \end{aligned} \tag{9}$$

with $B=PSFA_{tt}$.

Considering that $\lambda_2-\lambda_1=\Delta\lambda$, the phase shift associated with the modulation signal and the detected intensity can be expressed as follows

$$\varphi(\lambda_s)=\tan^{-1}\Big(\exp\Big(\alpha\,\Delta\lambda\,\Big(\frac{\lambda_1+\lambda_2}{2}-\lambda_s\Big)\Big)\Big) \tag{10}$$

$$\hat{I}(\lambda_s)=B\sqrt{\frac{\pi}{2\alpha}}\sqrt{\exp(-\alpha(\lambda_s-\lambda_1)^2)+\exp(-\alpha(\lambda_s-\lambda_2)^2)} \tag{11}$$

Therefore, any change on the sensor wavelength translates to a variation of the intensity and phase of the detected optical signal. As can be seen in Eq. (10), the phase is insensitive to the amplitude variations and it depends on the variation of λ_s. In this way, by measuring the signal phase shift the wavelength position of the sensor can be determined.

4. Results and discussion

4.1. Numerical results

By using the model outlined in the previous section, we analyzed the system when a FBG of 0.22 nm (FWHM) was employed. Several computations varying the spectral position of the FBG_1 and FBG_2 were carried out. The spectral position of the calibration Bragg gratings responds to the relations, $\lambda_1=1550-\Delta\lambda/2$ and $\lambda_2=1550+\Delta\lambda/2$.

In Fig. 2, phase plots computed using Eq. (10) were drawn for $\Delta\lambda=0.7$, 0.14, 0.2 and 0.33 nm, while intensity plots computed with Eq. 11 are shown in Fig. 3 for the same $\Delta\lambda$ values. Sensibilities for the phase detection, expressed in °/nm, are also shown in Fig. 4.

It can be noted that increasing $\Delta\lambda$, the detection sensitivity increases while the linear range decreases. For the greatest $\Delta\lambda$ values (0.33 nm) a diminishing of the intensity around 1550 nm is observed. By considering favorable cases of SNR, a relative phase of tenth of degree can be achieved in practice. In this case a 20°/nm sensitivity is equivalent to an error of 5 pm for the wavelength determination, while a sensitivity of 600°/nm allows to reach an error of 0.17 pm.

By selecting a FBG separation of $\Delta\lambda=0.33$ nm, a dynamic range of 0.25 nm is observed with variation in the detected intensity of 2 dB. In this example the useful range is limited by the phase linearity. The minimum and maximum sensitivities are 530 and 85°/nm equivalent to 0.2 and 1.2 pm wavelengths error, respectively. On the other hand, for $\Delta\lambda=0.07$ nm, the dynamic range is 0.45 nm, now limited by the intensity choosing a maximum variation of 6 dB. The minimum and maximum sensitivities are 120 and 85°/nm equivalent to 0.8 and 1.2 pm wavelength errors, respectively.

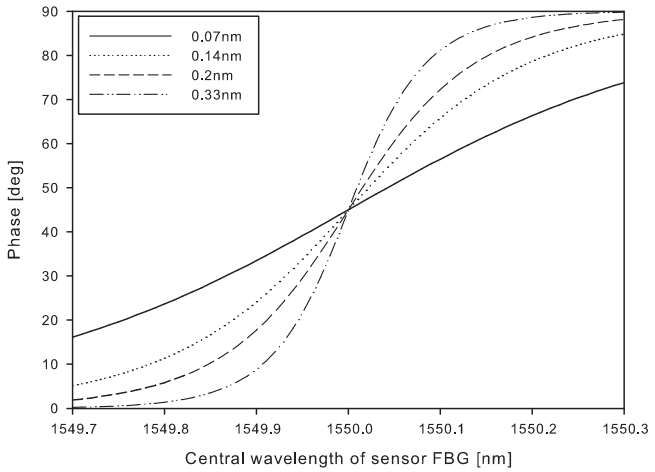

Fig. 2. Wavelength dependence of the phase for different spectral separation ($\Delta\lambda$) of calibration standard Bragg gratings.

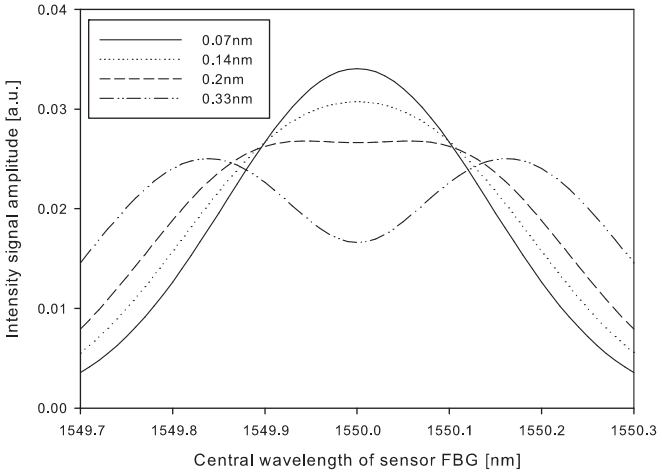

Fig. 3. Wavelength dependence of the signal amplitude for different spectral separation ($\Delta\lambda$) of calibration standards.

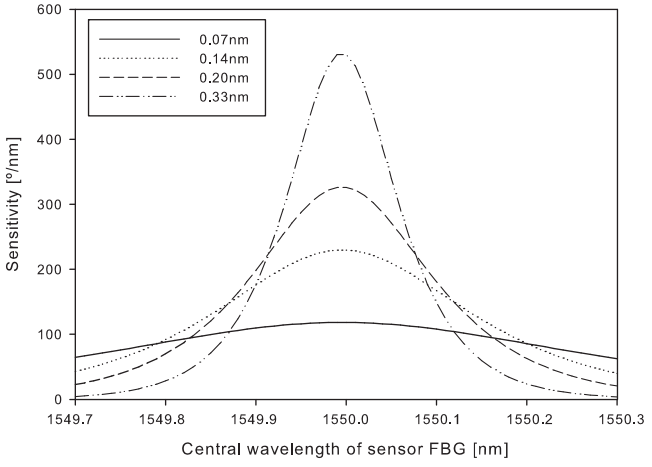

Fig. 4. Wavelength dependence of the phase sensitivity for different spectral separation ($\Delta\lambda$) of calibration standards.

4.2. Experimental results

Spectra of the FBG employed in the work, having a FWHM of 220 pm, are shown in Fig. 5. The modulation frequency ($f_c=23.5$ MHz) was adjusted so that the fiber length difference between the branches of the FBG pattern ($L\approx 3.2$ m) generate a 270° phase difference.

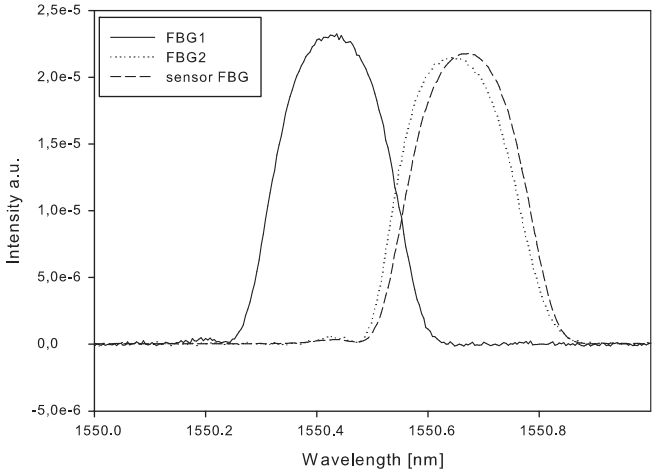

Fig. 5. Spectral characteristics of Bragg gratings used as sensor and as part of the interrogator device.

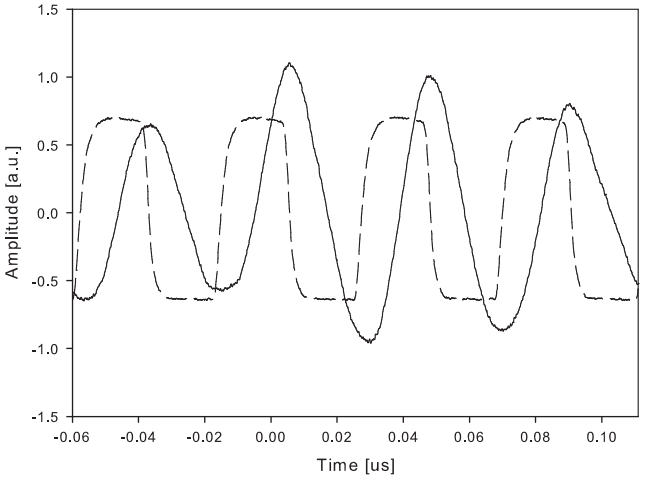

Fig. 6. Trigger (dashed line) and photodetected (solid line) signal.

The photodetected signal is shown in Fig. 6 superimposed to the signal used as phase reference for triggering the oscilloscope. The high modulation frequency allows to achieve high sample rates. The algorithm used for phase detection accumulates signal samples during 5 μs time intervals (more than a 100 of modulation cycles), so a output data rate of 200 kHz could be achieved. Another alternative approach is to accumulate more data to diminish noise effects and obtain better resolution at the expense of a lower data output rate.

The system was characterized for separation of calibration standards ($\Delta\lambda$) of: 70, 140, 200 and 330 pm. Phase and intensity of the detected signal are shown in Figs. 7 and 8, respectively. The wavelength axis was drawn relative to the middle wavelength between the calibration standards, assigned as the zero relative wavelength. Maximum sensitivities obtained are: 108, 255, 364 and 688°/nm.

As can be observed in Fig. 9, measured and theoretical data show good agreement. Some small differences appear due to the following reasons: (i) the different reflectivity of the calibration standard FBG's, (ii) the use of Gaussian spectrum shape for modeling the FBG and (iii) neither noise nor error source were considered in theoretical simulations. Far from zero relative wavelengths a significant difference between the Gaussian model and experimental results is in the phase response. It could be seen that phase falls down when sensor central relative wavelength modulus increases. We ascribe this behavior to spurious reflections that predominates on the

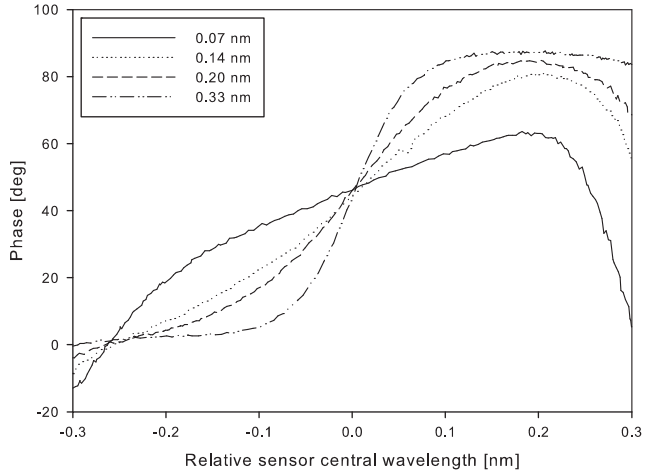

Fig. 7. System response: phase measured as a function of the sensor wavelength. Zero location corresponds to middle wavelength between the calibration standards. Maximum sensitivities are: 108, 255, 364 and 688°/nm.

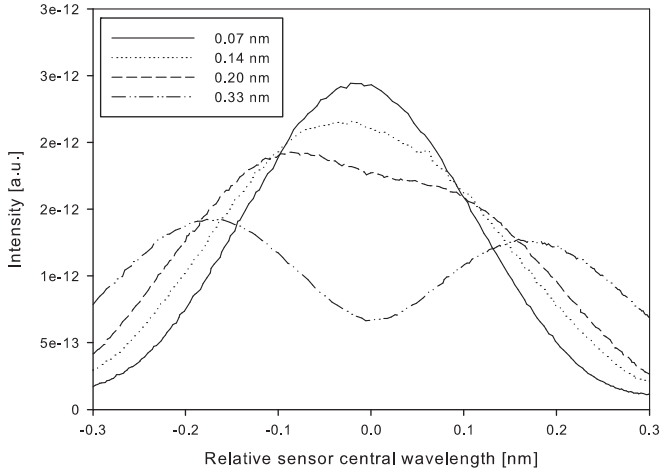

Fig. 8. System response: intensity as a function of the sensor wavelength. Zero location corresponds to middle wavelength between the calibration standards.

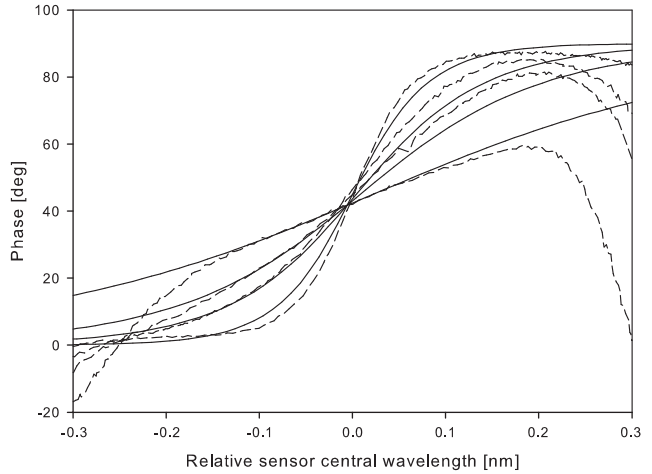

Fig. 9. Phase curves: Experimental data (dashed line) overlapped with theoretical data (solid line).

phase response when signal intensity decreases. When sensor spectrum goes away and it is not superimposed enough with FBG_1 or FBG_2 no light arrives to the photodetector with phase information related with the sensor. Reflections produced before

FBG_1 and FBG_2, such as that originated in some fiber connectors, arrive to the photodetector as a background always with the same phase independently of the sensor wavelength.

Finally, for the mentioned particular cases, the maximum sensitivity achieved from simulations were 530°/nm and 120°/nm for spectral separations between calibration standards of $\Delta\lambda = 0.33$ nm and $\Delta\lambda = 0.07$ nm, respectively. As a comparison, from the experimental results, sensitivities of 660 and 105°/nm were obtained for the same cases.

5. Conclusion

A simple interrogation technique for FBG sensors was discussed in this paper. This method combines low cost and high flexibility to be customized as required for a particular application. The scheme was based on a two fixed filters and a wavelength-time transformation procedure. A high correlation between the theoretical analysis and experimental results was obtained. A modulation frequency on the order of 20 MHz allows us to employ short fiber optics pieces to implement the necessary delay. System shows versatile customizable characteristics by changing the shape or the spectral position of the grating used as calibration standards. Moreover, by using adequate algorithms to process the signal, interrogation rates as high as 200 kHz can be reached. It is especially suitable to interrogate any application involving high frequency phenomena.

Acknowledgments

This work was supported by Consejo Nacional de Investigaciones Científicas y Técnicas (CONICET-PIP 112-201101-00397) and Facultad de Ingeniería de la Universidad Nacional de La Plata (UNLP, Project I169). A.A.G. thanks the UNLP for a fellowship.

References

[1] Kashyap R. Fiber Bragg gratings. second ed. San Diego, USA: Academic Press; 2009.
[2] Nunes LCS, Valente LCG, Braga AMB. Analysis of a demodulation system for Fiber Bragg Grating sensors using two fixed filters. Opt Lasers Eng 2004;42:529–42.
[3] John RN, Read I, MacPherson WN. Design considerations for a fibre Bragg grating interrogation system utilizing an arrayed waveguide grating for dynamic strain measurement. Meas Sci Technol 2013;24:075203–11.
[4] Oswald D, Richardson S, Wild G. Numerical modeling of interrogation systems for optical fibre Bragg grating sensors, smart nano-micro materials and devices. Proc SPIE 2011;82040Q-1–11 (Melbourne).
[5] Kim Ki-Soo, Chung Chul. Fiber Bragg grating sensor system for dynamic strain measurement without optical filters. Proc SPIE 2003;5050:152–8.
[6] Kersey AD, Berkoff TA, Morey WW. Multiplexed fiber Bragg grating strain-sensor system with a fiber Fabry–Perot wavelength filter. Opt Lett 1993;18:1370–2.
[7] Kersey AD, Berkoff TA, Morey WW. Fibre optic Bragg grating strain sensor with drift-compensated high-resolution interferometric wavelength shift detection. Opt Lett 1993;18:72–4.
[8] Zhou B, Guan Z, Yan Ch, He S. Interrogation technique for a fiber Bragg grating sensing array based on a Sagnac interferometer and an acousto-optic modulator. Opt Lett 2008;33(219):2485–7.
[9] Fu HY, Liu HL, Dong X, Tam HY, Wai PKA, Lu C. High-speed fibre Bragg grating sensor interrogation using DCF dispersion compensation fibre. Electron Lett 2008;44(10):618–9.
[10] Xia H, Blais S. Ultrafast and precise interrogation of fiber Bragg grating sensor based on wavelength-to-time mapping incorporating higher order dispersion. J Lightwave Technol 2010;28(3):254–61.
[11] Filograno ML, Corredera Guillén P, Rodríguez Barrios A, Martín López S, Rodríguez Plaza M, Andrés-Alguacil Á, Herráez MGonzález. Real-time monitoring of railway traffic using fiber Bragg grating sensors. IEEE Sens J 2012;12(1):85–92.
[12] Qi H., Liu T., Wang Ch., Wang J., Liu X. High sensitive multiplexed FBG microseismic monitoring system. IEEE symposium on photonics and optoelectronics. Wuhan; 2011.
[13] Abad S, Araújo FM, Ferreira LA, Santos JL, López-Amo M. Bragg-grating interrogation scheme using spectral filtering and amplitude-to-phase optical conversion. Opt Fiber Sens Conf Tech Dig 2002;1:103–6.